

Performance Assessment of Flat Plate Solar Collector Using Different Nanofluids

Mustafa Asker  Tukur Sani Gadanya 

Aydin Adnan Menderes University, Department of Mechanical Engineering, Aydin, Turkey

ABSTRACT

In this work, a numerical study has been performed to investigate the performance of a Flat plate solar collector (FPSC) using five different nanofluids including Al_2O_3 , CeO_2 , Cu, SiO_2 , and TiO_2 as the working fluid with a volume fraction (VF) range of 0-2% and mass flow rate of 0.02kg/s. A computer program written in MATLAB is developed and the equations are solved in an iterative approach to obtain the output temperature. The model is validated through a comparison with an experimental data that is taken from the literature and a good agreement is obtained. A parametric study is done to investigate the effects of VF's on the performance of the collector. The analyses have been conducted for the city of Aydin in Turkey. The results show that for VF of 2%, the maximum efficiency augmentation is observed in SiO_2 nanofluid by 10%.

Keywords:

Flat Plate Solar Collector; Nusselt Number; Thermal Performance; Nanofluid; Entropy

Article History:

Received: 2019/04/03

Accepted: 2019/08/23

Online: 2019/09/30

Correspondence to: Mustafa Asker
Aydin Adnan Menderes University,
Department of Mechanical Engineering
Tel: 0(256) 213 7503
Fax: 0(256) 213 6686
E-Mail: mustafa.asker@adu.edu.tr

INTRODUCTION

The need for renewable energy is gradually been recognized and accepted globally due to the threats the world is facing such as the increase in world population, climate change, fossil fuels price inflation and high cost of electricity. These threats have led to the discovery and development of new, clean and abundant alternative sources of energy called renewable energies. Among these alternative sources of energy includes solar, wind and hydropower.

Solar energy is a free, abundant and natural heat from the sun that is harnessed by solar collection method. It is the common alternative source of energy used today. It can be utilized directly in two forms: either to generate electricity by exposing a photovoltaic material to sunlight or to generate heat for heating or cooling system. For the heating system, the sun's radiation in the form of heat energy is transferred to a working fluid such as the air, water or oil. Use of solar energy for water heating is the most common and easiest application with the use of a solar collector with a flat plate been the most productive type [1]. Enhancing the heat transfer, by maximizing solar absorption and reducing the losses leads to improved efficiency and better performance. In addition, the use of nanofluids is another way for enhancing the performance of the collector. Sharafeldin et al. [2] conducted an experiment to study the effect of using CeO_2 with three different volume fractions (0.0167%,

0.0333% and 0.0666%) and a mean particle size of 30nm which was kept constant as the working fluid. They found that using CeO_2 nanofluid enhanced the efficiency compared to water. Kutlu et al. [3] investigated evacuated flat plate collector integrated with organic Rankine cycle. Their work focused on the system performance simulation for electrical production as well as water heating under different weather conditions. Verma et al. [4] conducted an experimental study using a variety of nanofluids to improve the performance of a FPSC in respect of energy and exergy efficiency by varying the mass flow rate. They found that for an optimum particle VF of 0.75% and mass flow rate of 0.025kg/s, the maximum exergetic efficiency is observed in multiwall carbon nanotubes (MWCNTs), Graphene, Cu, Al_2O_3 , TiO_2 and SiO_2 respectively. They concluded that the collector can be more frugal and efficient by reducing the collector surface area by about 19.11% as well as the use of MWCNTs nanofluid as the working fluid. In another work, Verma et al. [5] used MgO nanofluid as a working fluid. They showed that the thermal efficiency will be improved by 9.34% for 0.75% particle volume concentration. Sharafeldin [6] conducted an experiment to investigate the effect of using WO_3 on the thermal efficiency of a FPSC which operates under the weather condition of Budapest, Hungary. They found that usage of WO_3 nanofluid alleviates the thermal efficiency of the collector. Said et al. [7] used a controlled pH treated Al_2O_3

nanofluid as the working fluid to study its effects on the energetic and exeric efficiencies of a FPSC. An experiment was conducted and the results showed that for an optimum flow rate of 1.5kg/min and VF of 3%, the energetic efficiency increased by 83.5% whereas the exeric was enhanced by 20.3% for a VF of 1% and flow rate 1kg/min when compared with water. In another work, Said et al. [8] studied the thermophysical properties of Al_2O_3 nanofluid and its effect on the performance of a FPSC. They conducted an experiment to investigate the influence of density and viscosity on the pumping power using ethylene glycol/water and the Al_2O_3 . The result obtained showed that Al_2O_3 is preferred against sedimentation and agglomeration and that both their thermal conductivities increases with an increase in concentration. Yousefi et al. [9] performed an experiment to study the effect of using MWCNT and Triton X-100 as the surfactant. They found that for a VF of 2% without surfactant the efficiency decreases whereas, with a surfactant, it increases. Sabiha et al. [10] used single-walled carbon nanotube (SWCNT) to determine its effect on the thermal efficiency of an evacuated tube collector. They showed that the efficiency improved using the nanofluid in place of water as the working fluid. Hawwash et al. [11] developed a model by using ANSYS software to test the performance of FPSC using double distilled water (DDW) as well as Al_2O_3 nanofluid at different VF. They showed that the use of Al_2O_3 nanofluid enhances the efficiency compared to DDW by about 3-18% at both small and high temperature differences. Said et al. [12] used TiO_2 and Polyethylene Glycol (PEG) dispersant. Their results showed that for a constant mass flow rate of 0.5kg/min, both the energetic and exeric efficiencies increased by 76.6% and 16.9% respectively. Qinbo et al. [13] used Cu nanofluid to investigate the effects of working parameters such as temperature, heat gain, frictional resistance and thermal conductivity of the nanofluid on the efficiency of a FPSC. Their results show that for a constant flow rate of 140L/h, VF of 0.1% and particle size of 25nm, the thermal conductivity was enhanced as well as the efficiency by 23.83%. Mahian et al. [14] applied first and second law analysis to examine the efficiency of FPSC connected to minichannel using various nanofluids.

The integration of solar collection with a system is an area that recently received great attention. Bellos and Tzivanidis [15] applied multi objective optimization for FPSC integrated with an absorption chiller driven. They used Cu nanofluid as the working fluid and pure water. Their work indicated that utilizing the nanofluid improved the thermal efficiency up to 2.5%.

The use of nanofluid as the working fluid instead of water to improve the performance of the collector is gaining more attention. Different nanofluids have been studied by many researchers but few investigate which of the nanoflu-

Table 1. General collector specifications [16,17]

Collector parameters	Values
Length of collector	1.8 m
Width of the collector	1.2 m
Length of the absorber plate	1.65 m
Width absorber plate	1 m
Tilt angle θ	37°
Thickness δ	0.0005 m
Optical efficiency $\tau\alpha$	0.962
Centre distance between tubes W	0.1125 m
Number of covers	1
Diameter of riser pipes	0.0125 m
Diameter of header pipes	0.025 m
Back insulation thickness tb	0.04 m
Absorber plate emissivity of ϵ_p	0.07
Glass cover emissivity ϵ_g	0.88
Thermal conductivity of the absorber	386 W/m.K
Thermal conductivity of the insulation	0.044 W/m.K

ids would offer a better performance more than the others. This motivated the authors to investigate the performance of the collector using various nanofluids such as Aluminum oxide (Al_2O_3), Cerium oxide (CeO_2), Copper (Cu), Silicon oxide (SiO_2) and Titanium oxide (TiO_2) for various VF and mass flow rate. In addition, Entropy analysis is implemented to improve the performance of the system.

MATERIALS AND METHODS

Description Of The Problem

The FPSC system that is examined in this work is given in Fig. 1. When solar energy with intensity I incident drop on the outer layer of FPSC, part of it transmitted through the glazing and strikes the absorber plate. While the remaining part is dissipated to the surrounding as a heat loss. The tubes that are connected to the absorber, will be used to heat the working fluid as it passes inside the tubes. A pump is used to circulate the HTF inside the system. The general specifications of the collector are taken from [16, 17] and are summarized in Table 1. The analysis is done based on weather data for Aydın, Turkey.

The following assumptions are made for the analysis:

- A steady state system.
- The thermo-physical properties of the working fluids are constant.
 - The inlet temperature is constant and assumed to be $T_{amb} + 5$ K.
 - The guess temperature is assumed to be $T_{guess} = T_{in} + 10$ K.
- The Fluid flow inside the pipe is uniform.

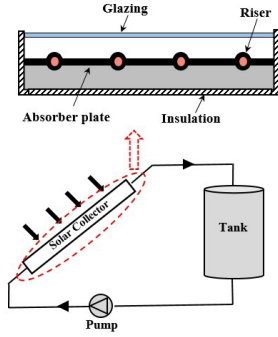


Figure 1. Schematic representation of FPSC system

The performance of a collector is expressed by applying an energy balance on FPSC. There are basically two types of losses that occur in a FPSC which are optical and thermal. The optical loss is shown as $I_T (\tau\alpha)$, where $(\tau\alpha)$ is the optical efficiency depending on the properties of the materials whereas the thermal loss is further divided into three i.e. top loss, bottom loss and edge loss [18].

The Overall heat loss U_L is the summation of the top, back and edge losses

$$U_L = U_t + U_b + U_e \quad (1)$$

Here, U_t can be evaluated as follows [18].

$$U_t = \left[\frac{N_{glass}}{\frac{C_1}{T_{abs}} \left[\frac{T_{abs} - T_{amb}}{N_{glass} + \lambda} \right]^{e_1} + h_{wind}} \right]^{-1} + \frac{\sigma(T_{abs} + T_{amb})(T_{abs}^2 + T_{amb}^2)}{(\epsilon_p + 0.0059N_{glass}h_{wind})^{-1} + \frac{2N_{glass} + \lambda - 1 + 0.133\epsilon_p - N_{glass}}{\epsilon_g}} \quad (2a)$$

Where:

$$\lambda = (1 + 0.089h_{wind} - 0.1166h_{wind}\epsilon_p)(1 + 0.07866N_{glass}) \quad (2b)$$

$$C_1 = 520(1 - \beta^2 0.000051) \quad (2c)$$

$$e_1 = 0.430 \left(1 - \frac{100}{T_{abs}} \right) \quad (2d)$$

The natural heat transfer coefficient caused by wind is given as [18]

$$h_{wind} = 5.7 + 3.8V_{wind} \quad (3)$$

The back and edge heat losses can also be determined as [18]

$$U_b = \frac{k_b}{t_b} \quad (4)$$

$$U_e = \left(\frac{k_e}{t_e} \right) \frac{A_e}{A_c} \quad (5)$$

Where k_e and k_b are thermal conductivities of the back and edge insulation respectively, A_e is the edge surface area, t_e and t_b are the thickness of edge and back insulations respectively.

The useful energy output can be written as [18]

$$Q_u = F_R A_c [I_T (\tau\alpha) - U_L (T_i - T_{amb})] \quad (6)$$

F_R denote the heat removal factor and expressed in Eq. (7) [18].

$$F_R = \frac{\dot{m}c_p}{A_c U_L} \left[1 - \exp \left(\frac{-U_L F' A_c}{\dot{m}c_p} \right) \right] \quad (7)$$

Where F' is collector efficiency factor defined as

$$F' = \frac{1/U_L}{W \left[\frac{1}{[U_L(D_o + (W - D_o)F)] + \frac{1}{C_b} + \frac{1}{\pi D_i h_{fi}}} \right]} \quad (8)$$

Where F is the f_{in} efficiency defined as

$$F = \frac{\tanh[m(W - D_o)/2]}{m(W - D_o)/2} \quad (9)$$

Where

$$m = \sqrt{\frac{U_L}{k_c \delta_c}} \quad (10)$$

HEAT TRANSFER IN FPSC

For water as the working fluid, the Gnielinski Correlation [19] is used to calculate the Nusselt number.

$$Nu = \frac{\left(\frac{f}{8}\right)(Re - 1000)Pr}{1 + 12.7\left(\frac{f}{8}\right)^{0.5}\left(Pr^{\frac{2}{3}} - 1\right)} \quad 0.5 \leq Pr \leq 2000 \quad (11)$$

The Internal heat transfer coefficient is expressed in term of Nusselt number as

$$h_{fi} = \frac{Nu k}{D_i} \quad (12)$$

For nanofluid as the working fluid, Xuan and Li correlation [20, 21] is used to evaluate Nu for $0 \leq \phi \leq 2$

If the flow is laminar ($Re_{nf} < 2300$).

$$Nu_{nf} = 0.4328 \left(1 + 11.285\phi^{0.754} (Re_{nf} \times Pr_{nf})^{0.218} \right) \times Re_{nf}^{0.333} Pr_{nf}^{0.4} \quad (13)$$

If turbulent flow ($Re_{nf} \geq 4000$).

$$Nu_{nf} = 0.0059 \left(1 + 7.6286 \phi^{0.6886} (\text{Re}_{nf} \times \text{Pr}_{nf})^{0.001} \right) \times \text{Re}_{nf}^{0.9238} \text{Pr}_{nf}^{0.4} \quad (14)$$

Where Re_c , Pr stands for Reynolds and Prandtl numbers respectively and are given below.

$$\text{Re} = \frac{4\dot{m}}{\pi D_i \mu} \quad (15)$$

$$\text{Pr} = \frac{\mu c_p}{k} \quad (16)$$

The correlation used to evaluate the k of nanofluids is adapted from [22].

$$k_{nf} = \left[\frac{k_p + 2k_w + 2(k_p - k_w)(1+b)^3 \phi}{k_p + 2k_w - (k_p - k_w)(1+b)^3 \phi} \right] k_w \quad (17)$$

Brinkman [23] suggested an equation to compute the viscosity of the nanofluid as

$$\mu_{nf} = \frac{1}{(1-\phi)^{2.5}} \mu_w \quad (18)$$

The nanofluid density and specific heat are evaluated by using Pak and Cho [24] correlation.

$$\rho_{nf} = \phi \rho_p + (1-\phi) \rho_w \quad (19)$$

$$c_{p,nf} = \frac{\rho_w c_{p,w} (1-\phi) + \rho_p c_{p,p} \phi}{\rho_{nf}} \quad (20)$$

In this study, five different nanofluids which include aluminium oxide (Al_2O_3), cerium oxide (CeO_2), copper (Cu), silicon oxide (SiO_2) and titanium oxide (TiO_2) are used. The thermo-physical properties of the working fluids are listed in Table 2.

A computer program written in MATLAB is used to get the outlet temperature. A moderate value for T_{abs} must be assumed as an initial guess through which U_L , F_R as well as Q_u are obtained. The T_{abs} is calculated by using Eq. (21) and the guessed value is corrected by an iterative approach [18].

Table 2. Thermo-physical properties of nanoparticles [2, 14]

Particle	c_p (J/kg.K)	k (W/m.K)	ρ (kg/m ³)
Al_2O_3	765	40	3970
TiO_2	686	8.9	4250
SiO_2	745	1.4	2220
CeO_2	4175	0.624	999
Cu	385	400	8933
Water	4180	0.6068	997.07

$$T_{\text{abs}} = T_m + \frac{Q_u}{A_c F_R U_L} (1 - F_R) \quad (21)$$

$$\left| \frac{(T_{\text{abs}})_{\text{guess}} - (T_{\text{abs}})_{\text{calculated}}}{(T_{\text{abs}})_{\text{calculated}}} \right| \leq 10^{-8} \quad (22)$$

The outlet temperature is obtained as follow [18]

$$T_{\text{out}} = T_{\text{in}} + \frac{Q_u}{\dot{m} c_p} \quad (23)$$

The thermal efficiency can be expressed as [25].

$$\eta_{\text{en}} = \frac{Q_u}{A_c I_r + \text{Pumping Power}} \quad (24)$$

The total entropy generation [26].

$$\dot{S}_{\text{gen}} = \dot{m} c_p \ln \frac{T_{\text{out}}}{T_{\text{in}}} - \frac{\dot{Q}_s}{T_s} + \frac{\dot{Q}_o}{T_{\text{amb}}} \quad (25)$$

Where, \dot{Q}_s and \dot{Q}_o are the heat absorbed (W) by the collector surface and heat lost to the surrounding (W) respectively.

$$\dot{Q}_s = I_r \eta_o A_c \quad (26)$$

$$\dot{Q}_o = \dot{Q}_s - \dot{m} c_p (T_{\text{out}} - T_{\text{in}}) \quad (27)$$

Pressure Drops

The pressure drop for the FPSC is calculated as follow [27].

$$\Delta P = \left[f \frac{L}{D_i} \left(\rho \frac{V^2}{2} \right) \right]_{\text{in/out header}} + \left[\rho g (L \sin(\beta) + h_L) \right]_{\text{riser+ fittings}} \quad (28)$$

where, h_L represents the total head loss which consist of two parts major and minor losses, is given as follow [28].

$$h_L = \frac{8 \dot{m}^2}{\rho^2 g \pi^2 D_i^4} \left(f \frac{L}{D_i} + \sum K \right) \quad (29)$$

The term f given in Eq. (29) represent the frictional factor which can be evaluated by using Goudar-Sonnad correlation [29]. The reason behind using this correlation is that, it is non-iterative and more accurate [30].

RESULTS AND DISCUSSION

A numerical model has been conducted to investigate the impact of various type nanofluids on the performance of FPSC. In addition, energy analysis is done and the pressure drop is evaluated for different values of mass flow rate and solar radiation. In order to validate the numerical model of this work, the result are compared with experimental data obtained by [15]. The numerical model is observed to be in good agreement with the published work from [15] which make the works reliable as shown in Fig. 2.

Throughout the solution, the solar load is selected as 562 W/m² [31]. Also, wind velocity is taken as 2 m/s [32], $T_{\text{amb}}=308$ K [32] and kg/s with the use of the collector spe-

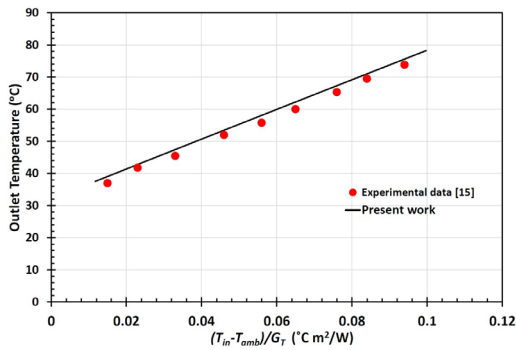


Figure 2. Comparison of outlet temperature with Ref. [15].

cification that is mentioned in Table 1.

Fig. 3 shows the impact of particle VF increase and its influence on the heat transfer performance. In this figure, for Cu nanofluids with 0% VF, the value of $Nu=11.7605$ and $h_{fi}=570.9 \text{ W/m}^2 \cdot \text{K}$ based on Eq. (13) and Eq. (14). While for water the value of $Nu=14.0159$ and $h_{fi}=680.3897 \text{ W/m}^2 \cdot \text{K}$. by using Eq. (11) and Eq. (12) respectively. Since the convective heat transfer coefficient is proportional to both Nu and thermal conductivity, the it is improved as the VF increases. A maximum increase is observed at VF of 2% in Al_2O_3 . This is obvious, because during particle loading, both the k and μ of the base fluid are augmented. However, the rise in thermal conductivity results to better heat transfer performance whilst increase in viscosity results to development in boundary layer thickness. For the VFs used, the effect of thermal enhancement is higher than that of viscosity. Therefore, the heat transfer increases.

The variation of outlet temperature with VF is shown in Fig. 4. In this figure, at a given value of volume fraction Cu nanofluid provides the maximum outlet temperature whereas SiO_2 nanofluid shows the smallest value. Based on Eq. (23), the outlet temperature is inversely proportional to the heat capacity. By definition, specific heat is the heat required to raise the temperature of a unit mass of a substance by one unit of temperature i.e. the smaller the heat capacity the higher the outlet temperature. Other factors such as density and thermal conductivity also determines higher

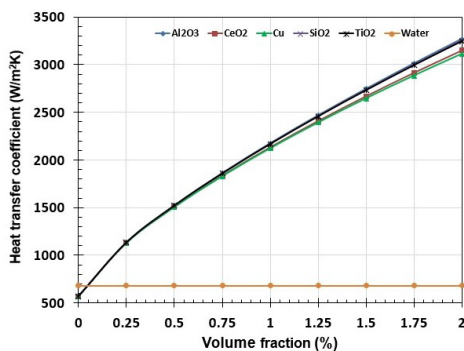


Figure 3. Heat transfer coefficients with respect to VF for different nanofluids.

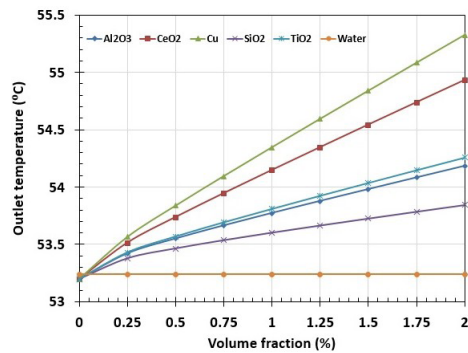


Figure 4. Outlet temperatures against VF for different nanofluids.

outlet temperature. Al_2O_3 shows higher outlet temperature than SiO_2 despite having less heat capacity. The reason is, for a constant mass flow rate, a nanofluid with higher density results to lower velocity which makes it easier to absorb higher thermal energy. Moreover, Al_2O_3 having higher thermal conductivity. The maximum outlet temperature is observed on Cu, CeO_2 , TiO_2 , Al_2O_3 and SiO_2 respectively for VF of 2%. However, the maximum outlet temperature is $55.32 \text{ }^\circ\text{C}$ at 2% VF of Cu.

Fig. 5 depicts the change of thermal efficiency with VF. In this figure, the opposite trend to the outlet temperature with SiO_2 nanofluid providing the highest efficiency whereas Cu nanofluid the smallest. This happened because among all the nanofluids, Cu provides the highest absorber plate temperature and the absorbed energy will be minimized. Therefore, the efficiency reduced. Moreover, the thermal efficiency is a function of VF to a certain limit. The maximum efficiency improvement is “between” 0.75% to 2% for all the working fluids. Besides, the maximum efficiency is observed in SiO_2 by 10%.

To develop an efficient thermal system, entropy generation analysis will play a vital role. Fig. 6 describes the influence of VF on entropy generation. At a given condition, the total entropy generation is diminished by using nanofluid with water. This is because; addition of nanoparticles increases the transfer of heat efficiently due to the augmentation in the value of k for nanofluids. Thus, the irreversibility generated in the system is depressed. The maximum drop

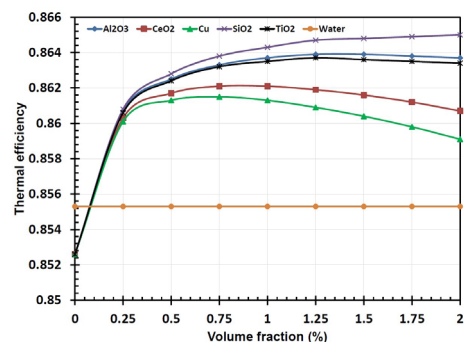


Figure 5. Thermal efficiency against VF for different nanofluids.

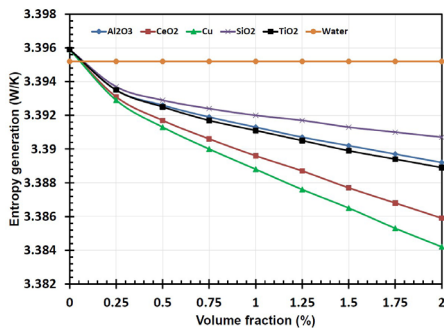


Figure 6. Entropy generation against VF.

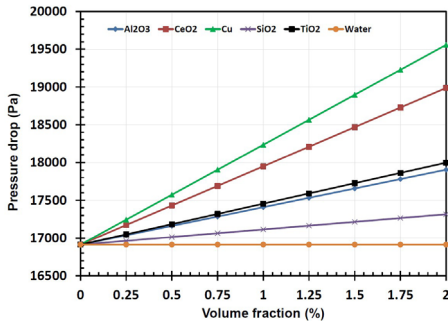


Figure 7. Pressure drop variation with respect to VF.

in entropy generation is observed in Cu, followed by CeO₂, then TiO₂, Al₂O₃ and lastly SiO₂.

Fig. 7 illustrates the variation of pressure drop against the VF for different nanofluids. In this figure, the supplementation of nanoparticles into the water improves its viscosity which results to increase in the frictional factor. It can be seen that at VF=2 for Cu nanofluid the pressure drop is 19559 Pa while for SiO₂ nanofluid is 17315 Pa. As a result, the pressure drop rises with the increasing concentration.

In Figs. 8-10 different values of mass flow rate such as 0.01, 0.02 and 0.03 kg/s are selected to examine its effect on outlet temperature, thermal efficiency and pressure drop correspondingly. the solar radiation and the volume fraction for nanofluids are taken as 562 W/m² and 1.25 respectively.

Fig. 8 exhibits the distributions of outlet temperature for various mass flow rates for different nanofluids. The highest outlet temperature occurs in lowest mass flow rate.

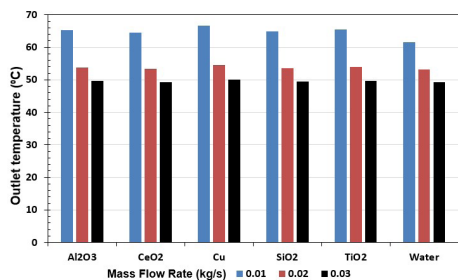


Figure 8. Variation of outlet temperature for different mass flow rate.

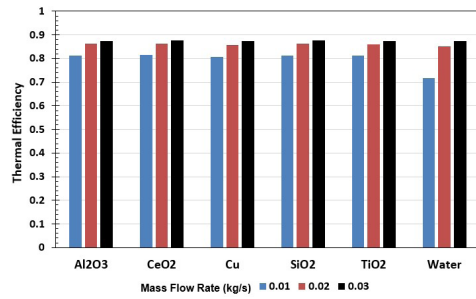


Figure 9. Variation of thermal efficiency for different mass flow rate.

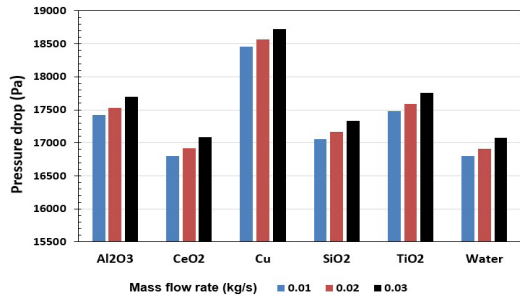


Figure 10. Variation of pressure drop for different mass flow rate.

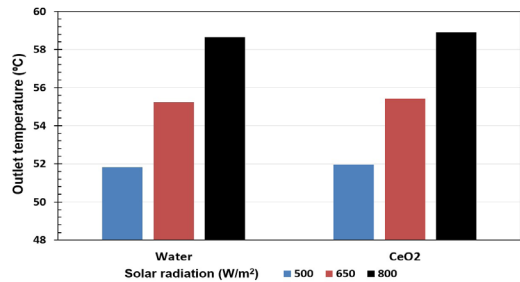


Figure 11. Variation of outlet temperature for different solar radiation.

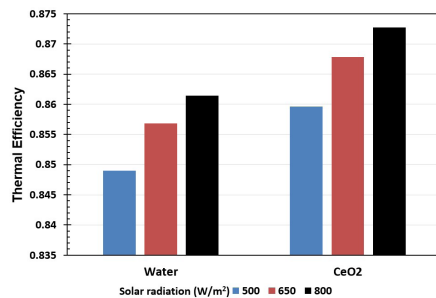


Figure 12. Variation of thermal efficiency for different solar radiation.

In Fig. 9, on the other hand the variation of thermal efficiency is given for different mass flow rate. At maximum value of mass flow rate leads to higher thermal efficiency rates. This because, as the mass flow rate increase the useful energy output will be increased based on equation (6). Therefore, higher thermal efficiency will be obtained according to Eq. (24).

Fig. 10 illustrates the pressure drop for the various nanofluid for different mass flow rate. Increasing the mass flow rate leads to an increase in pressure drop due to direct

proportion of pressure drop with fluid velocity (Equation 28). In addition, the nanofluid exhibiting the highest-pressure drop is copper (Cu).

The effect of solar radiation on the performance of solar collector and pressure drop is analysed. To perform these analyses, cerium oxide (CeO_2) is selected. The mass flow rate for the HTF and the VF for nanofluids are taken as 0.02 kg/s and 1.25 respectively. In addition, three different solar loads (500 W/m^2 , 650 W/m^2 , 800 W/m^2) are selected. Fig. 11 illustrates the variation of outlet temperature for different solar radiation for different nanofluid. As can be seen in Fig. 11, the highest solar radiation results in higher outlet temperature.

Fig. 12 shows the distribution of thermal efficiency for various solar radiation for different nanofluid. As can be seen in Fig. 12, the highest solar radiation lead to an increase in thermal efficiency because of the increase in useful energy output according to Equation (6). Increasing the solar radiation from 500 W/m^2 to 800 W/m^2 with the same flat plate collector area causes the thermal efficiency rate for CeO_2 to increase from 86% to 87.3%.

CONCLUSION

In this study, a computational analysis of FPSC is implemented to investigate the influence of using five different nanofluids which includes Al_2O_3 , CeO_2 , Cu, SiO_2 and TiO_2 for different VF's. Moreover, the influence of mass flow rate for heat transfer fluid (HTF) and solar radiation are also investigated.

We believe that this study is useful for the various thermal design applications.

The following are the results of the study summarized below:

- 1- Al_2O_3 nanofluid shows the highest heat transfer coefficient whereas Cu the smallest.
2. Cu nanofluid provides the highest outlet temperature followed by CeO_2 , TiO_2 , Al_2O_3 and SiO_2 .
3. SiO_2 provides higher thermal efficiency enhancement by up to 10% compared to water at 0.02 kg/s and VF of 2%.
4. Increasing the VF diminishes entropy generation value with maximum drop observed in Cu, CeO_2 , TiO_2 , Al_2O_3 and SiO_2 nanofluids respectively.
5. FPSC with VF of 2% has higher pressure drop which seen in Cu, CeO_2 , TiO_2 , Al_2O_3 and SiO_2 respectively.

Nomenclature

A_c	Collector surface area (m^2)
A_e	Edge surface area (m^2)
c_p	Specific heat (J/kg.K)

D_o	Outer diameter of the collector tube (m)
D_i	Inner diameter of the collector tube (m)
F	Fin efficiency
F'	Collector efficiency factor
f	Frictional factor
g	Gravitational acceleration (m/s^2)
G_T	Incident solar radiation (W/m^2)
I	Heat flux of solar radiation (W/m^2)
k	Thermal conductivity (W/m.K)
L	length (m)
\dot{m}	Mass flow rate (kg/s)
N_{glass}	Number of the glass cover
Nu	Nusselt number
P	Pressure (Pa)
Pr	Prandtl number
Qu	Absorbed energy by plate (W)
Re	Reynolds number
\dot{S}_{gen}	Entropy generation (W/K)
T	Temperature (K)
T_{abs}	Absorber temperature (K)
T_{amb}	Ambient temperature (K)
T_p	Plate temperature of (K)
t_b	Back thickness (m)
te	Edge thickness (m)
V_{wind}	Wind velocity (m/s)
W	Tube spacing (m)

Greek symbols

α	Absorption coefficient
β	Collector inclination angle (degree)
μ	Viscosity of fluid (kg/m.s)
δ_c	Thickness of absorber plate (m)
ε	Emissivity
ρ	Density (Kg/m^3)
σ	Stefan-Boltzmann constant ($\text{W}/(\text{m}^2.\text{K}^4)$)
$\tau\alpha$	Optical efficiency
ϕ	Volume fraction of nanofluids

Subscripts

p	Particles
w	Water
nf	Nanofluid
in	Inlet
out	Outlet

Abbreviations

FPSC	Flat plate solar collector
HTF	Heat transfer fluid
VF	Volume fraction

REFERENCES

1. Alima MA, Abdin Z, Saidur R, Hepbasli A, Khairul MA, Rahim NA. Analyses of entropy generation and pressure drop for a conventional flat plate solar collector using different types of metal

- oxide nanofluids. *Energy and Buildings* 66 (2013) 289-296.
2. Sharafeldin MA, Grof G. Experimental investigation of flat plate solar collector using CeO₂ nanofluid. *Energy Conversion and Management*, 155 (2018) 32-41.
 3. Kutlu C, Li J, Su Y, Wang Y, Pei G, Riffat S. Annual Performance Simulation of a Solar Cogeneration Plant with Sensible Heat Storage to Provide Electricity Demand for a Small Community: A Transient Model. *Hittite Journal of Science and Engineering*, 6 (2019) 75-81.
 4. Verma S K, Tiwari AK, Chauhan DS. Experimental evaluation of flat plate solar collector using nanofluid. *Energy Conversion and Management* 134 (2017) 103-115.
 5. Verma, SK, Tiwari AK, Chauhan DS. Performance agumentation in flat plate solar collector using MgO/water nanofluid. *Energy Conversion and Management* 124 (2016) 607-617.
 6. Sharafeldin MA, Grof G, Mahian O. Experimental study on the performance of a flat plate collector using WO₃/Water nano fluids. *Energy* 141 (2017) 2436-2444.
 7. Said Z, Saidur R, Sabiha MA, Hepbasli A, Rahim NA. Energy and exergy efficiency of a flat plate solar collector using pH treated Al₂O₃ nanofluid. *Journal of Cleaner Production*, 112 (2016) 3915-3926.
 8. Said Z, Sajid MH, Alim MA, Saidur R, Rahim NA. Experimental investigation of the thermophysical properties of AL₂O₃-nanofluid and its effect on a flat plate solar collector. *International Communications in Heat and Mass Transfer* 48 (2013) 99-107.
 9. Yousefi T, Farzad V, Ehsan S, Sirus Z. An experimental investigation on the effect of MWCNT-H₂O nanofluid on the efficiency of flat-plate solar collectors. *Experimental Thermal and Fluid Science* 39 (2012) 207-212.
 10. Sabiha MA, Saidur R, Hassani S, Said Z, Mekhilef S. Energy performance of an evacuated tube solar collector using single walled carbon nanotubes nanofluids. *Energy Conversion and Management* 105 (2015) 1377-1388.
 11. Hawwash AA, Abdel Rahman AK, Nada SA, Ookawara S. Numerical Investigation and Experimental Verification of Performance Enhancement of Flat Plate Solar Collector Using Nanofluids. *Applied Thermal Engineering* 130 (2018) 363-374.
 12. Said Z, Sabiha MA, Saidur R, Hepbasli A, Rahim NA, Mekhilef S, Ward TA. Performance enhancement of a Flat Plate Solar collector using Titanium dioxide nanofluid and Polyethylene Glycol dispersant. *Journal of Cleaner Production* 92 (2015) 343-353.
 13. He Q, Zeng S, Wang S. Experimental investigation on the efficiency of flat-plate solar collectors with nanofluids. *Applied Thermal Engineering* 88 (2015) 165-171.
 14. Mahian O, Kianifar A, Sahin AZ, Wongwises S. Performance analysis of a minichannel-based solar collector using different nanofluids. *Energy Conversion and Management* 88 (2014) 129-138.
 15. Bellos E, Tzivanidis C. Performance analysis and optimization of an absorption chiller driven by nano fluid based solar flat plate collector. *Journal of Cleaner Production* 174 (2018) 256-272.
 16. Gunjo GD, Manhanta P, Robi PS. CFD and experimental investigation of flat plate solar water heating system under steady state condition. *Renewable Energy* 106 (2017) 24-36.
 17. Shojaeizadeh E, Veysi F, Kamandi A. Exergy efficiency investigation and optimization of an Al₂O₃/water nanofluid based Flat-plate solar collector. *Energy and Buildings* 101 (2015) 12-23.
 18. Duffie JA, Beckman WA. *Solar Engineering of Thermal Processes*, fourth ed. Wiley, New Jersey, 2013.
 19. Gnielinski V. New equations for heat and mass transfer in turbulent pipe and channel flow. *International Chemical Engineering* 16 (1979) 359-368.
 20. Xuan Y, Li Q. Investigation on convective heat transfer and flow features of nanofluids. *Journal of Heat Transfer* 125 (2003) 151.
 21. Sint N KC, Choudhury IA, Masjuki HH, Aoyama H. Theoretical analysis to determine the efficiency of a CuO-water nanofluid based-flat plate solar collector for domestic solar water heating system in Myanmar. *Solar Energy* 155 (2017) 608-619.
 22. Yu W, Choi SUS. The role of interfacial layers in the enhanced thermal conductivity of nanofluids: a renovated Maxwell model. *Journal of Nanoparticle Research* 5 (2003) 167-171.
 23. Brinkman HC. The viscosity of concentrated suspensions and solution. *The Journal of Chemical Physics* 20 (1952) 571.
 24. Pak BC, Cho YI. Hydrodynamic and heat transfer study of dispersed fluids with submicron metallic oxide particles. *Experimental Heat Transfer* 11 (1998) 151-170.
 25. Genc MA, Ezan MA, Turgut A. Thermal performance of a nanofluid-based flat plate solar collector: A transient numerical study. *Applied Thermal Engineering*, 130 (2018) 395-407.
 26. Bejan A. *Entropy Generation Minimization: the Method of Thermodynamic Optimization of Finite-size Systems and Finite-time Processes*, first ed. CRC Press, Florida, 1996.
 27. White FM. *Fluid Mechanics*. 7th ed. McGraw-Hill, Boston, 2009.
 28. Shamsirgaran S, Assadi KM, Al-Kayiem H, Sharma KV. Energetic and Exergetic Performance of a Solar Flat-Plate Collector Working with Cu Nanofluid. *Journal of Solar Energy Engineering*, 140 (2018) 031002.
 29. Goudar CT, Sonnad JR. Comparison of the iterative approximations of the Colebrook-White equation, *Hydrocarbon Processing*, 87 (2008) 79-83.
 30. Asker M, Turgut O E, Coban MT. A review of non-iterative friction factor correlations for the calculation of pressure drop in pipe. *Bitlis Eren University Journal of Science and Technology*, 4 (2014) 1-8.
 31. Photovoltaic Geographical Information System. <http://re.jrc.ec.europa.eu/pvgis/apps4/pvest.php> (08.07.2018)
 32. Turkish State Meteorological Service. <https://www.mgm.gov.tr/> (08.07.2018)